Observation of Weak-Limit Quasiparticle Scattering via Broadband Microwave Spectroscopy of a *d*-Wave Superconductor

P. J. Turner, R. Harris, Saeid Kamal, M. E. Hayden,* D. M. Broun,* D. C. Morgan, A. Hosseini, P. Dosanjh, G. K. Mullins, J. S. Preston,† Ruixing Liang, D. A. Bonn, and W. N. Hardy

Department of Physics and Astronomy, University of British Columbia, Vancouver, British Columbia, Canada V6T 1Z1

(Received 31 July 2002; published 13 June 2003)

There has long been a discrepancy between microwave conductivity measurements in high temperature superconductors and the conductivity spectrum expected in the simplest models for impurity scattering in a *d*-wave superconductor. Here we present a new type of broadband measurement of microwave surface resistance that finally shows some of the spectral features expected for a $d_{x^2-y^2}$ pairing state. Cusp-shaped conductivity spectra, consistent with weak impurity scattering of nodal quasiparticles, were obtained in the 0.6–21 GHz frequency range in highly ordered crystals of $YBa_2Cu_3O_{6.50}$ and $YBa_2Cu_3O_{6.99}$.

DOI: 10.1103/PhysRevLett.90.237005 PACS numbers: 74.25.Nf, 74.72.Bk

It is now widely accepted that superconductivity in the cuprates involves a pairing state with $d_{x^2-y^2}$ symmetry [1]. This ground state is one of the simplest features of a phase diagram that continues to confound attempts at an overall understanding. The question is, despite the new physics being encountered in the cuprates, to what extent can conventional Bardeen-Cooper-Schrieffer theory describe the superconducting state? Well below T_c, most properties *ought* to be controlled by quasiparticle excitations near the nodes of the $d_{x^2-y^2}$ gap function. In particular, the key signatures of nodal-quasiparticle transport appear in the *frequency dependence* of $\sigma_1(\omega, T)$, the in-plane microwave conductivity. Until now, there has been a disturbing inconsistency between measurements of $\sigma_1(\omega, T)$ and theoretical models for impurity-dominated scattering [2]. To specifically address this question, we have developed a highly sensitive broadband microwave spectrometer, one that will find broad applicability to other condensed matter systems. In this Letter, we present $\sigma_1(\omega, T)$ measurements that reveal for the first time the cusp-shaped spectra expected for weak-limit impurity scattering in a clean *d*-wave superconductor. These characteristic spectra have remained elusive because they appear only at temperatures far below T_c in very clean crystals where measurements of the residual microwave absorption are most challenging.

The low-energy density of states of a clean $d_{x^2-y^2}$ superconductor is expected to have the form $N(\varepsilon) \propto \varepsilon/\Delta_0$ due to the linear dispersion of the superconducting gap near its nodes in momentum space. At sufficiently low T, $\sigma_1(\omega, T)$ should be governed by the nodal quasiparticle excitations. The microscopic details of the scattering mechanism and the framework for calculating the conductivity provide an opening where novel physics might enter into the problem. In the low T limit, the conventional framework is a self-consistent *t*-matrix approximation (SCTMA) developed to account for impurity pair-breaking effects which modify both $N(\varepsilon)$ and the electron self-energy [3,4]. This work showed that the microwave conductivity expression for any scattering strength takes a simple energy-averaged Drude form $\sigma(\omega, T) = ne^2/m^\star\langle[i\omega + \tau^{-1}(\varepsilon)]^{-1}\rangle_\varepsilon$, where the energy dependence of the scattering rate $\tau^{-1}(\varepsilon)$ is determined by the strength of the scattering and $\langle\cdots\rangle_\varepsilon$ denotes a thermal average weighted by $N(\varepsilon)$ [3]. At low T, the unitary (strong-scattering) limit result has $\tau^{-1}(\varepsilon) \approx \Gamma_u/\varepsilon$ while the Born limit has $\tau^{-1}(\varepsilon) \approx \Gamma_B\varepsilon$ (to within logarithmic corrections), where the scale factors Γ_u and Γ_B are determined by the impurity density. The puzzling failure of this theory has been that neither form resembles the energy-independent τ^{-1} inferred from the microwave measurements on $YBa_2Cu_3O_{6.99}$ by Hosseini *et al.* [2].

Two major technical steps have now led to the discovery of a low T regime where some of the expectations of the simple theory seem to hold. First, the samples used here are of exceptionally high crystalline perfection. Most cuprate materials retain substantial intrinsic disorder due to cation cross substitution, but the $YBa_2Cu_3O_{6+x}$ system has a chemical stability that guarantees extremely low cation disorder ($< 10^{-4}$). Large improvements in the purity of $YBa_2Cu_3O_{6+x}$ crystals followed the advent of $BaZrO_3$ crucibles, which do not corrode during crystal growth [5]. With a very high degree of atomic order in the CuO_2 planes, the secondary disorder effect of the off-plane oxygen atoms becomes important. Since intercalated oxygen in the CuO chains in this material (which run along the $\hat{b}$ axis) acts as the reservoir for hole doping, probing the phase diagram typically involves nonstoichiometry and off-plane disorder. However, a few highly ordered phases are available in this system. Here we concentrate on fully doped $YBa_2Cu_3O_7$, with every CuO chain filled, and ortho-II ordered $YBa_2Cu_3O_{6.50}$, with alternate CuO chains filled. The perfection of the fully doped samples is limited to $O_{6.99}$ by not being able to anneal to completely full chains. The crystalline

perfection of the $YBa_2Cu_3O_{6.50}$ crystals comes from the high purity which in turn allows the development of very long correlation lengths of ortho-II order ($\xi_a = 148$ Å, $\xi_b = 430$ Å, and $\xi_c = 58$ Å) [6]. For the present work we used mechanically detwinned single crystals of 99.995% purity with dimensions $(a \times b \times c) \sim (1 \times 1 \times 0.010)$ mm^3.

The second key step is a bolometric method of detection, which provides a natural way of covering the microwave spectrum in more detail than is possible with a set of fixed-frequency experiments. The technique has recently proven useful for measuring resonant absorption in the cuprates [7]. For the present work we have improved the sensitivity of the technique to the pW level necessary for resolving the intrinsic power absorption of a small single crystal, while employing an *in situ* Ag:Au alloy reference sample of known surface resistance that calibrates the absorption absolutely. This is particularly important because it compensates for the strong frequency dependence of the microwave field amplitude caused by standing waves in the microwave circuit.

The microwave surface resistance $R_s(\omega, T)$ is inferred from the synchronous measurement of the sample temperature rise as the amplitude of the microwave magnetic field $\vec{H}_{\rm rf}$ is modulated at low frequency (1 Hz). The high-T_c and reference samples are placed in symmetric positions in a rectangular shaped coaxial transmission line with a broadened center conductor designed to ensure spatial magnetic field homogeneity (inset of Fig. 1). The coaxial line is terminated with a short, providing a region where the samples experience predominantly magnetic fields. Both samples are mounted on thin sapphire plates with a small amount of silicone grease. Chip heaters on the thermal stages allow precise calibration of the thermal sensitivity, while the use of a second Ag:Au sample in place of the high-T_c sample confirms the absolute value and frequency independence of the calibration. All measurements use the low demagnetization factor geometry for a thin platelet, with $\vec{H}_{\rm rf} \parallel \hat{b}$. Thus the screening currents run along the crystal's $\hat{a}$ axis, completing the loop with a short section of $\hat{c}$-axis current which we do not attempt to correct for but know to be a small contribution.

Figure 1 shows $R_s(\omega, T)$ for $\hat{a}$-axis currents in a crystal of $YBa_2Cu_3O_{6.50}$. The measurements span 0.6–21 GHz, limited at low frequency where the small dissipation of the sample approaches the resolution limit of the experiment. The 1 GHz values for the rms uncertainty in R_s, δR_s, are about 0.2, 0.4, 0.6, and 1.3 $\mu\Omega$ for $T = 1.3$, 2.7, 4.3, and 6.7 K, respectively. For the worst case of 6.7 K this translates to $\delta\sigma_1/\sigma_1 = 0.14$ with uncertainties decreasing correspondingly at higher frequencies and lower temperatures. For clarity, error bars are omitted from the figures. At high frequencies, the apparatus is limited by deviations from the TEM field configuration in the sample region. An overall 5% uncertainty in R_s is set mainly by the Ag:Au reference-alloy dc resistivity measurement.

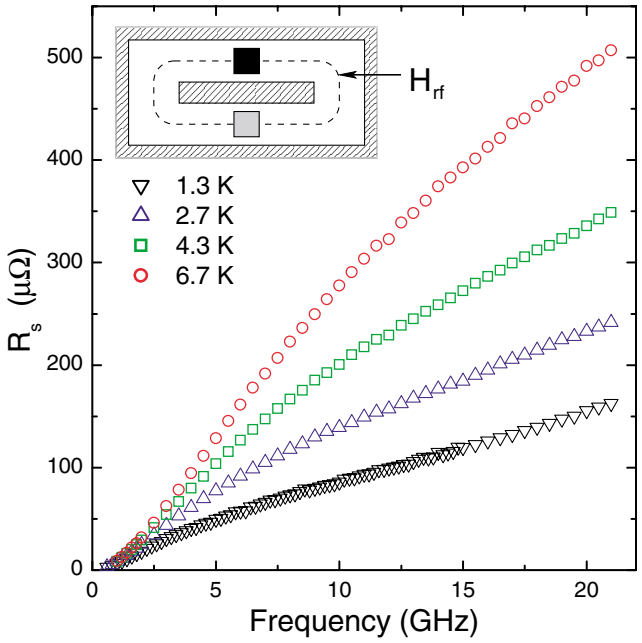

FIG. 1 (color online). Low T surface resistance data for the $\hat{a}$-axis direction of ortho-II ordered $YBa_2Cu_3O_{6.50}$ from synchronous power absorption measurements. A cross section of the microwave transmission line used is shown in the inset, with the platelet-shaped high T_c (black) and Ag:Au alloy reference (grey) samples positioned in regions of homogeneous $\vec{H}_{\rm rf}$.

In the local electrodynamic limit, relevant for our sample geometry [8], the surface impedance $Z_s = R_s + iX_s$ is related to the conductivity $\sigma = \sigma_1 - i\sigma_2$ via $Z_s = \sqrt{i\mu_0\omega/\sigma}$. Measurements of both R_s and X_s can be used to determine σ_1 and σ_2, but broadband measurements of only R_s present a problem. A common solution, used in infrared measurements, is to measure a single quantity such as reflectance over a wide enough range that Kramers-Kronig and Fresnel equations can be used to calculate σ_1 and σ_2. Another solution is to fit spectra to a model that automatically satisfies the Kramers-Kronig relations. Deep in the superconducting state, microwave measurements allow another option for extracting $\sigma_1(\omega, T)$ from $R_s(\omega, T)$ since both σ_2 and X_s are controlled by the superfluid screening. At low frequency, $X_s = \mu_0\omega\lambda$ and $\sigma_2 = (\mu_0\omega\lambda^2)^{-1}$ where λ is the London penetration depth. So, at low T a broadband measurement of $R_s(\omega, T)$ together with a measurement of $\lambda(T)$ at a single frequency is sufficient to extract $\sigma_1(\omega, T)$. Using cavity perturbation techniques with a superconducting loop-gap resonator operating at 1.1 GHz [9], we measure $\Delta X_s(T) = \mu_0\omega\Delta\lambda(T)$, where $\Delta\lambda(T) = \lambda(T) - \lambda(1.2\ {\rm K})$ is the T dependent increase of the London penetration depth from its low T limit. Since these measurements do not determine λ absolutely, we take the $T \to 0$ value to be $\lambda_0 = 1600$ Å for $YBa_2Cu_3O_{6.99}$ from infrared reflectance [10] and $\lambda_0 = 2600$ Å for $YBa_2Cu_3O_{6.50}$, from μSR measurements [11]. A more accurate extraction of $\sigma_1(\omega, T)$ involves a

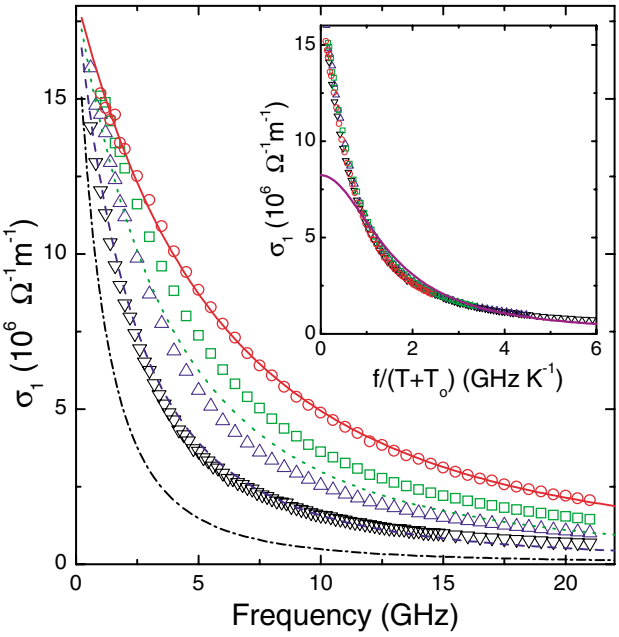

FIG. 2 (color online). The low T evolution of the quasiparticle conductivity spectra of ortho-II $YBa_2Cu_3O_{6.50}$ (same symbols as Fig. 1). The solid curve is a fit to the 6.7 K data with the Born-scattering model, but the dashed curves show that the model fails to capture the observed T dependence. The inset shows that the data obey an unusual frequency-temperature scaling $\sigma_1(\omega, T) = \sigma_1(\omega/[T + T_0])$ with $T_0 = 2.0$ K. The Drude fit in the inset illustrates the inadequacy of the Lorentzian line shape.

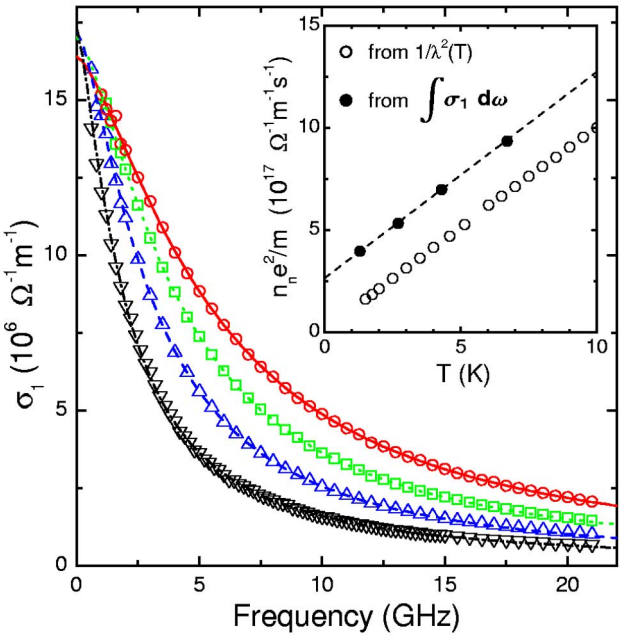

FIG. 3 (color online). Phenomenological fits with Eq. (1) (same symbols as Fig. 1). The inset compares the normal fluid density $n_n e^2/m^\star$ obtained by integrating Eq. (1) with the loss of superfluid density inferred from 1.1 GHz $\Delta\lambda(T)$ data. The dashed line has the slope of the open symbols, and the agreement indicates that the normal-fluid and superfluid spectral weight obey the conductivity sum rule, although a residual normal fluid term is implied.

correction for screening by the normal fluid. To do this we use a self-consistent method that includes contributions to $\sigma_2(\omega, T)$ both from the superfluid and from the quasiparticles [2]. At the low temperatures of this experiment, where there are few quasiparticles, this is a small correction having a maximum effect of 8% on σ_1 for our highest temperatures and frequencies.

Figure 2 depicts the real part of the quasiparticle conductivity extracted from the broadband R_s measurements. The strong frequency dependence over intervals as small as 1 GHz (0.05 K) shows that the time scale associated with the scattering of low-energy quasiparticles in these extremely clean samples falls within our bandwidth. The cusplike shape of $\sigma_1(\omega, T)$, the approximately T-independent low frequency limit and a tail that falls more slowly than $1/\omega^2$ are all features expected for Born scattering. The solid curve in Fig. 2 shows a convincing fit to the 6.7 K data using the energy-averaged Drude form with $\tau^{-1}(\varepsilon) = \Gamma_B\varepsilon$, indicating that the overall shape of the spectrum is well-described by the weak scattering calculation with fit parameters $\hbar\Gamma_B = 0.032$ and $ne^2\hbar/(m^\star\Delta_0) = 5.9 \times 10^5\ \Omega^{-1}\,\mathrm{m}^{-1}$. The other curves are the Born-limit predictions for the lower temperatures, using the parameters that fit the 6.7 K data. Clearly this model progressively underestimates the spectral weight as T is reduced, and thus a global fit for all temperatures produces less satisfactory results. The inset of Fig. 2 shows that the $\sigma_1(\omega, T)$ data scale as $\omega/(T + T_0)$ with $T_0 = 2.0$ K, rather than scaling as ω/T as expected in the Born-limit. Hence, the weak scattering limit captures the spectral line shape, but the SCTMA model's requirement that the spectral weight vanish as $T \to 0$ leads to disagreement.

To fit the spectra, we adopt a phenomenological form for $\sigma_1(\omega, T)$ that captures the Born-line-shape features, namely, the cusplike shape and high frequency tail:

$$\sigma_1(\omega, T) = \sigma_0/[1 + (\omega/\Gamma)^y]. \quad (1)$$

We fit directly to $R_s(\omega, T)$, thereby automatically accounting for the quasiparticle screening. Figure 3 shows the fits to individual spectra using this model where the parameters σ_o and y remain relatively constant, taking average values of $1.67(\pm 0.05) \times 10^7\ \Omega^{-1}\,\mathrm{m}^{-1}$ and $1.45(\pm 0.06)$, respectively. The parameter Γ varies approximately linearly in T with fit values 12.1, 19.2, 26.3, and $35.0 \times 10^9\ \mathrm{sec}^{-1}$. Although these fits also suggest the unusual ω–T scaling discussed previously, enforcing it in the model reduces the agreement in the spectral weight comparison. Integration of the fits provides the *absolute* T dependent spectral weight associated with the normal fluid. In the inset of Fig. 3 this normal fluid spectral weight is compared to the spectral weight lost from the superfluid as determined independently by the measurements of $\Delta\lambda(T)$. The slopes agree to within

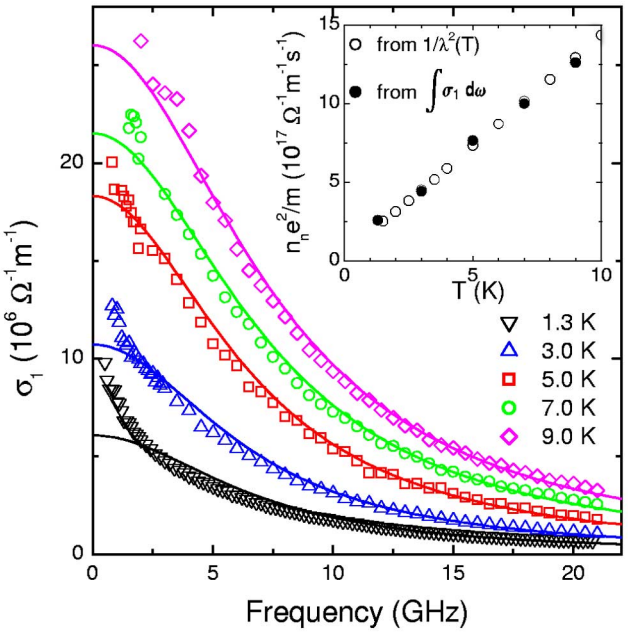

FIG. 4 (color online). The conductivity spectrum of a fully doped sample of $YBa_2Cu_3O_{6.99}$ in the $\hat{a}$ direction. The Drude fits to the spectra highlight the evolution from a cusplike shape to a more Lorentzian line shape with increasing temperature.

2%, a good indication that the model captures the oscillator strength at higher frequencies. We emphasize that at low T this comparison is independent of the choice of λ_0 to first order since $\sigma_1 \approx 2R_s/(\mu_0^2\omega^2\lambda_0^3)$ and $\Delta(1/\lambda^2) \approx -\Delta\lambda/\lambda_0^3$. The offset apparent in the normal fluid density corresponds to a $T = 0$ residual normal fluid.

The discovery of a cusp-shaped spectrum for the low temperature conductivity of $YBa_2Cu_3O_{6.50}$ seems at odds with the Drude fits [$y = 2$ in Eq. (1)] that were found to reasonably describe the spectra inferred from fixed-frequency microwave measurements on fully doped $YBa_2Cu_3O_{6.99}$ [2]. To resolve this conflict, broadband measurements were made on a crystal of the fully doped material, shown in Fig. 4. At the lowest T there is indeed a cusplike spectrum, similar to the ortho-II case. This was not seen in earlier measurements because the spectrum gives way to a more Lorentzian line shape above 4 K, as indicated by the progressively better fit to a Drude model with increasing T; the five spectra do not scale in the manner seen for $YBa_2Cu_3O_{6.50}$. Hosseini *et al.* concluded that τ^{-1} reaches a T independent value of $5.6(\pm 0.6) \times 10^{10}$ s^{-1} below 20 K, and here we find $\tau^{-1} = 4.4(\pm 0.3) \times 10^{10}$ s^{-1} with the decrease likely due to continued improvements in sample purity. Integrating the Drude model captures the oscillator strength rather well, except at the lowest T where the fits are too poor for us to comment upon an extrapolated residual value. It is not yet clear why the non-Lorentzian line shapes are restricted to such low T in the fully doped sample.

In summary, we have provided the first highly detailed measurements of the quasiparticle conductivity spectrum in the disorder-dominated regime of an extremely clean d-wave superconductor. This regime has been accessed by using well-ordered crystals with very high purity, measured with a broadband microwave technique whose frequency range matches the very small quasiparticle scattering rate in the samples. A number of puzzles remain, particularly the residual normal fluid inferred from extrapolations to $T = 0$, a phenomenon that is seen to a much greater degree in other cuprates [12,13]. The cause of the evolution from a cusplike spectrum to a more Lorentzian line shape in $YBa_2Cu_3O_{6.99}$ is also unclear and may require a more sophisticated model that employs intermediate scattering strengths. Nevertheless, several features *are* characteristic of Born-limit scattering, namely, a cusp-shaped conductivity spectrum seen at low T. Additional physics such as order parameter suppression at impurity sites [14] might be needed to resolve the remaining puzzles, but the data presented here provide a simple starting point that is quite close to the expectation for weakly scattered nodal quasiparticles.

We gratefully acknowledge useful discussions with A. J. Berlinsky, C. Kallin, and P. J. Hirschfeld, and financial support from the Natural Science and Engineering Research Council of Canada and the Canadian Institute for Advanced Research.

*Permanent address: Department of Physics, Simon Fraser University, Burnaby, B.C., Canada, V5A 1S6.
†Permanent address: Department of Physics and Astronomy, McMaster University, Hamilton, ON, Canada, L8S 4M1.

[1] C. C. Tsuei and J. R. Kirtley, Rev. Mod. Phys. **72**, 969 (2000).
[2] A. Hosseini *et al.*, Phys. Rev. B **60**, 1349 (1999).
[3] P. J. Hirschfeld, W. O. Putikka, and D. J. Scalapino, Phys. Rev. Lett. **71**, 3705 (1993); Phys. Rev. B **50**, 10 250 (1994).
[4] C. T. Rieck, D. Straub, and K. Scharnberg, J. Low Temp. Phys. **117**, 1295 (1999).
[5] A. Erb, E. Walker, and R. Flukiger, Physica (Amsterdam) **258C**, 9 (1996); R. X. Liang, D. A. Bonn, and W. N. Hardy, Physica (Amsterdam) **304C**, 105 (1998).
[6] R. X. Liang, D. A. Bonn, and W. N. Hardy, Physica (Amsterdam) **336C**, 57 (2000).
[7] Y. Matsuda *et al.*, Phys. Rev. B **49**, 4380 (1994); O. K. C. Tsui *et al.*, Phys. Rev. Lett. **73**, 724 (1994); M. Gaifullin *et al.*, Phys. Rev. Lett. **83**, 3928 (1999).
[8] I. Kosztin and A. J. Leggett, Phys. Rev. Lett. **79**, 135 (1997).
[9] W. N. Hardy *et al.*, Phys. Rev. Lett. **70**, 3999 (1993).
[10] D. N. Basov *et al.*, Phys. Rev. Lett. **74**, 598 (1995).
[11] R. I. Miller *et al.* (unpublished).
[12] D. M. Broun *et al.* (unpublished).
[13] J. Corson *et al.*, Phys. Rev. Lett. **85**, 2569 (2000).
[14] M. H. Hettler and P. J. Hirschfeld, Phys. Rev. B **61**, 11313 (2000).